Physica E 59 (2014) 218–222

Contents lists available at ScienceDirect

Physica E

journal homepage: www.elsevier.com/locate/physe

Synthesis of single crystalline $(NH_4)_2V_6O_{16}\cdot 1.5H_2O$ nest-like structures

Pallellappa Chithaiah [a], Gangaiah Vijaya kumar [a], Gowdaiahnapallya Puttaiah Nagabhushana [a], Ganganagappa Nagaraju [b], Gujjarahalli Thimmanna Chandrappa [a,*]

[a] Department of Chemistry, Bangalore University, Bangalore 560001, India
[b] Laboratory of Molecular Catalysis, Institute of Chemistry, UFRGS, Porto Alegre, Brazil

HIGHLIGHTS

- Nest-like $(NH_4)_2V_6O_{16}\cdot 1.5H_2O$ structures have been facilely synthesized.
- A hydrothermal method has been employed.
- A reaction mechanism for the formation of $(NH_4)_2V_6O_{16}\cdot 1.5H_2O$ structures is discussed.

ARTICLE INFO

Article history:
Received 19 July 2013
Received in revised form
26 December 2013
Accepted 28 December 2013
Available online 20 January 2014

Keywords:
Hydrothermal
Micro-architecture
Nanobelt
Crystal growth
V_2O_5.

ABSTRACT

Novel nest-like $(NH_4)_2V_6O_{16}\cdot 1.5H_2O$ structures made of nanobelts have been synthesized by a facile hydrothermal approach. The powder X-ray diffraction pattern of the sample reveals the monoclinic crystalline phase of $(NH_4)_2V_6O_{16}\cdot 1.5H_2O$. The scanning electron microscopy images of the sample obtained at 130 °C for 3 days exhibit nest-like morphology. The transmission electron microscopy result reveals that the nanobelts have a smooth surface. The selected area electron diffraction pattern of the nanobelts indicates single crystalline nature. The two major weight losses occur in thermogravimetric analysis which correspond to the removal of water and ammonia molecules. Further, calcination of the $(NH_4)_2V_6O_{16}\cdot 1.5H_2O$ product results in the formation of orthorhombic phase of shcherbianite V_2O_5.

1. Introduction

Over the past few years, considerable attention has been devoted to the synthesis of one-dimensional (1D) nanostructured materials such as nanotubes, nanorods, nanowires and nanobelts, because of their novel physical and chemical properties [1–3]. Among various metal oxide nanostructures, one-dimensional vanadium oxide-based nanostructured materials have interested many researchers over the last few decades due to their outstanding structural flexibility [4], diverse technological applications in catalysis [5,6], rechargeable lithium ion batteries [7], chemical sensors or actuators [8,9], electrochemical pseudo-capacitors [10] and electro-chromic coatings [11]. Several synthesis methods, such as thermal evaporation, surfactant-assisted solution, hydrothermal and solvothermal have been employed to prepare 1-D nanostructured vanadium oxides and their compounds [12–16]. However, there have been a few reports on the synthesis of 1-D nanostructured single crystalline vanadates. For example, Durupthy et al. synthesized the crystalline $NaV_3O_8\cdot 1.5H_2O$ at room temperature on acidification of a metavanadate solution [17]. Yu et al. and Zhou et al. have synthesized $Na_2V_6O_{16}\cdot 3H_2O$ nanobelts and nanowires in the presence of F^- and SO_4^{2-} anions, respectively [18,19]. Mai et al. reported the synthesis, electrical transport measurements, and conduction mechanism on nanobelts of $NH_4V_3O_8$ vanadate [20]. Wang et al. reported that the one-dimensional ammonium vanadates are semiconductors at room temperature [2]. More recently, we reported the synthesis of $Na_2V_6O_{16}\cdot 3H_2O$ belts/rings and suggested that the $Na_2V_6O_{16}\cdot 3H_2O$ rings were made of self-coiling nanobelts [21]. However, it is still a big challenge for materials scientists to fabricate 1D nanostructured materials through a simple and facile route. In the present study, we report the synthesis of nest-like $(NH_4)_2V_6O_{16}\cdot 1.5H_2O$ architectures made of nanobelts by the hydrothermal method and the possible reaction mechanism for the formation of $(NH_4)_2V_6O_{16}\cdot 1.5H_2O$ architecture is discussed. The orthorhombic phase of shcherbianite V_2O_5 is obtained on calcination of $(NH_4)_2V_6O_{16}\cdot 1.5H_2O$ at 350 °C for 2 h.

* Corresponding author. Tel.: +91 80 22961350.
E-mail address: gtchandrappa@yahoo.co.in (G.T. Chandrappa).

1386-9477/$ - see front matter © 2014 Elsevier B.V. All rights reserved.
http://dx.doi.org/10.1016/j.physe.2013.12.022

2. Experimental

2.1. Synthesis

All reagents were of analytical grade and used as received without further purification. Distilled water was used throughout. 0.5 g of NH_4VO_3 (4.27×10^{-3} mol) powder was added into 25 mL of distilled water and 0.2 mL of orthophosphoric acid (H_3PO_4, 88%, pH ~ 1.5) was also added, resulting in the formation of a wine red solution. The solution was stirred for about 15 min and transferred to a 60 mL Teflon lined stainless steel autoclave, which was maintained at 130 °C for 3 days and then cooled to room temperature. The red product was collected and washed with distilled water and absolute alcohol and then dried at 60 °C for 2 h.

2.2. Characterization

Powder X-ray diffraction (PXRD) data were recorded on a Philips X'pert PRO X-ray diffractometer with graphite-monochromatized Cu Kα radiation ($\lambda = 1.541$ Å) operated at 40 kV and 30 mA. The Fourier transform infrared (FTIR) spectrum of the sample was collected using a Thermo Nicolet FTIR spectrometer. The water content in the sample was investigated by thermogravimetric analysis (TGA) using a SDT Q600 thermomicrobalance in N_2 atmosphere from room temperature to 600 °C at a heating rate of 10 °C min^{-1}. The morphologies of the products were examined by a Quanta-200 scanning electron microscope (SEM) equipped with an energy dispersive X-ray spectroscopy (EDX). The nano-/microstructure of the product was observed by transmission electron microscopy (TEM) and selected area electron diffraction (SAED) which were performed with a Hitachi model H-600 instrument operating at 100 kV.

3. Results and discussion

The PXRD pattern of the as-prepared sample is shown in Fig. 1a. All the diffraction peaks in the pattern can be readily indexed to a pure monoclinic crystalline phase of $(NH_4)_2V_6O_{16} \cdot 1.5H_2O$ (JCPDS Card no. 51-0376). No reflections of impurity are found in the pattern, which proves that pure $(NH_4)_2V_6O_{16} \cdot 1.5H_2O$ has been successfully synthesized.

The FTIR spectrum of the as-prepared sample is shown in Fig. 1b. The bands at 1004 cm^{-1} and 964 cm^{-1} correspond to V=O stretching of distorted octahedral and distorted square-pyramids respectively; the bands at 733 and 534 cm^{-1} are ascribed to asymmetric and symmetric stretching vibrations of V–O–V bonds. The two bands at 3501 and 1617 cm^{-1} are attributed to O–H stretching and H–O–H bending vibrations of water molecules respectively. The bands at 3154 and 1402 cm^{-1} are respectively assigned to the

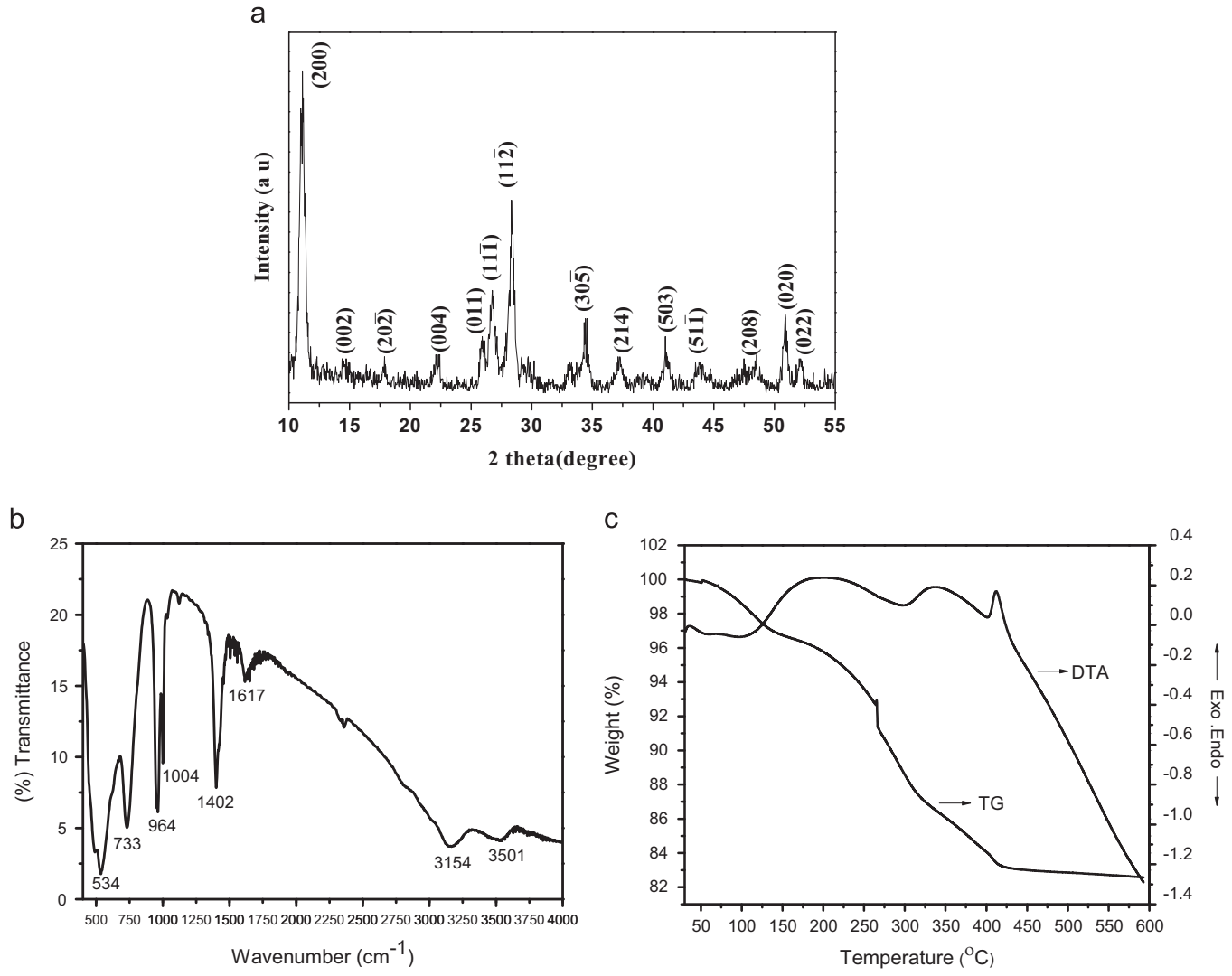

Fig. 1. (a) PXRD pattern (b) FTIR spectrum and (c) TG-DTA curves of $(NH_4)_2V_6O_{16} \cdot 1.5H_2O$.

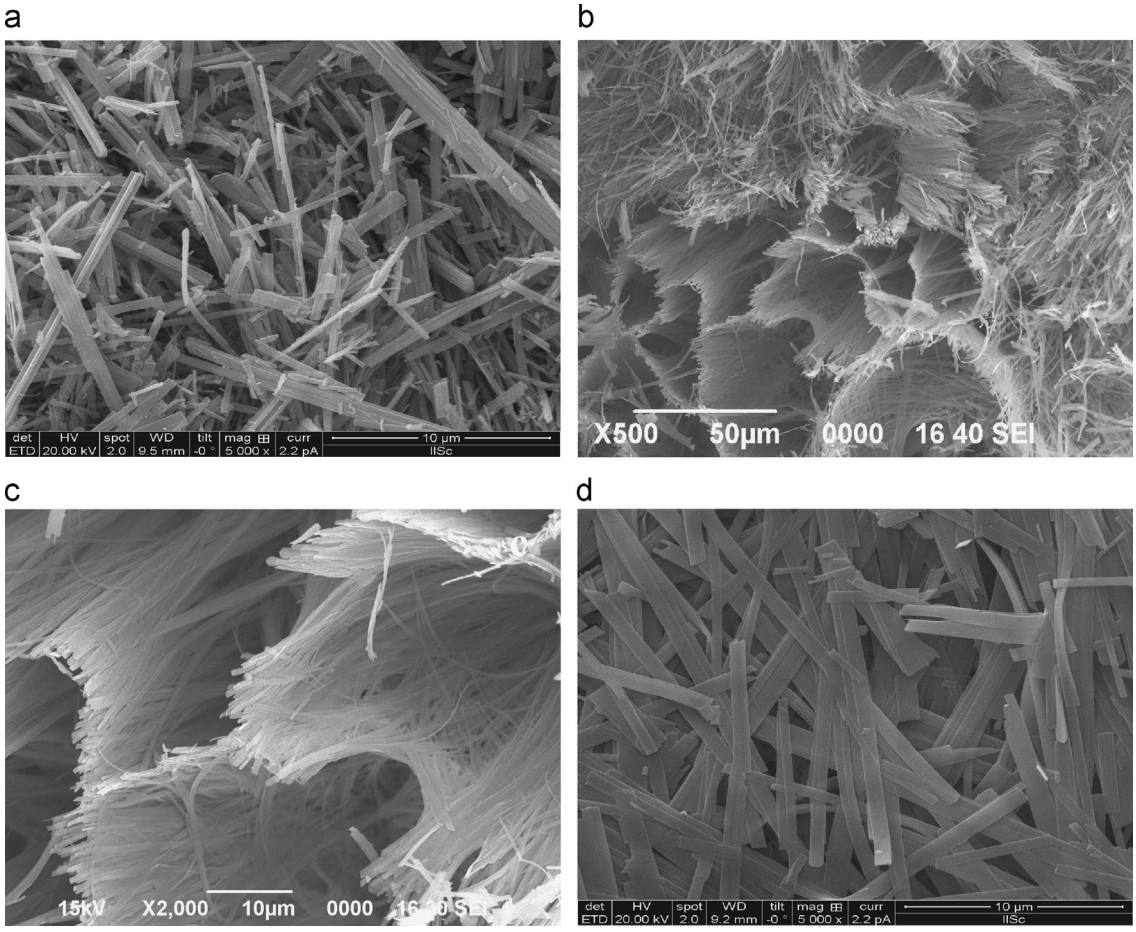

Fig. 2. SEM images of the $(NH_4)_2V_6O_{16}\cdot 1.5H_2O$ product prepared at (a) 120 °C, 24 h; (b) 130 °C, 3 days; low magnification (c) 130 °C, 3 days; high magnification (d) 160 °C, 3 days.

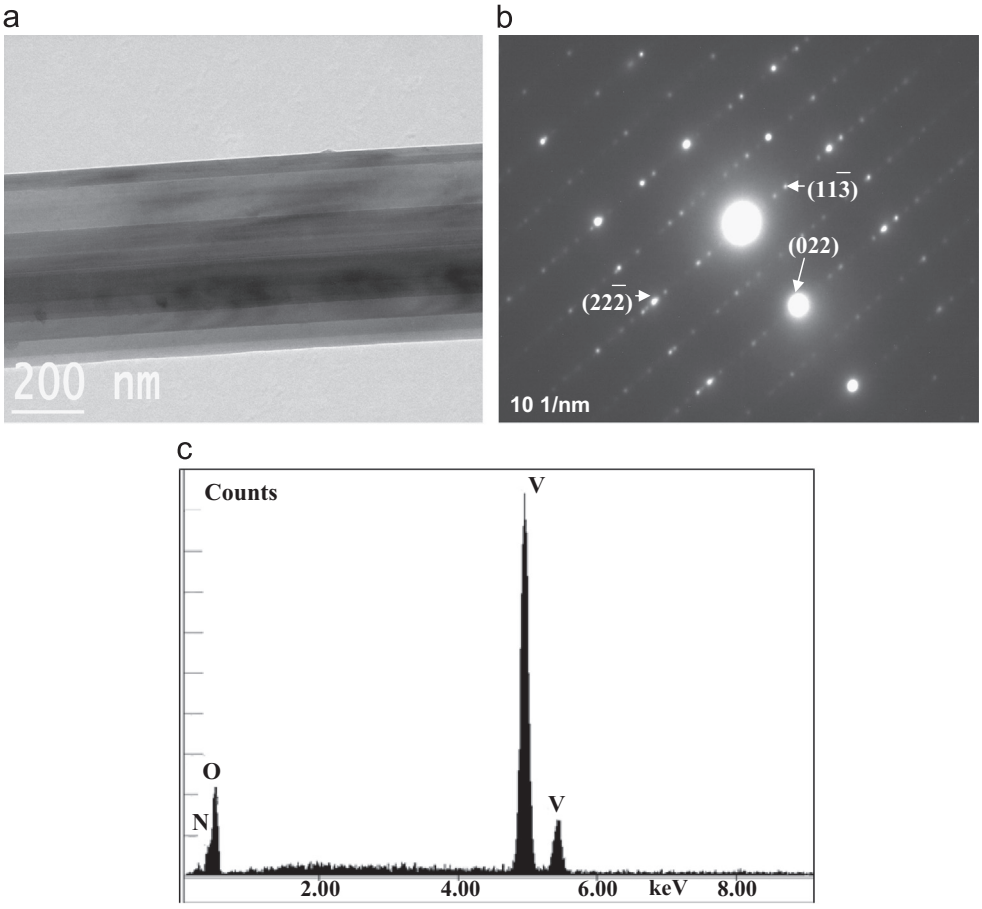

Fig. 3. (a) TEM image (b) SAED pattern of an individual $(NH_4)_2V_6O_{16}\cdot 1.5H_2O$ nanobelt and (c) EDX spectrum of $(NH_4)_2V_6O_{16}\cdot 1.5H_2O$.

asymmetric stretching and the symmetric bending vibrations of NH_4^+ [20].

The TG-DTA curves of the as-prepared sample are shown in Fig. 1c. The first weight loss of 5.6% from 100°C to 255 °C mainly resulted from the evaporation of NH_3 and water. The second weight loss of 8.0% from 260 to 375 °C was caused by the de-intercalation of strongly-bounded water. The exothermic peak at 412 °C can be assigned to the oxidation of V (IV) to V (V) [22].

The morphology and structure of the $(NH_4)_2V_6O_{16}\cdot 1.5H_2O$ product were investigated by SEM and TEM. The product obtained at 120 °C for 1 day (Fig. 2a) does not indicate any regular, well-defined shaped structure and is composed of a mixture of nanorods and nanobelts. When the experiment was performed at 130 °C for 3 days, the product exhibits nest-like morphology made of nanobelts (Fig. 2b and c). When the reaction was performed at 160 °C for 3 days (Fig. 2d), the dispersed nanobelts were obtained. The obtained nanobelts have the smooth surface with an average width of 300–400 nm and the length of several tens of micrometers. Fig. 3a shows the TEM image of selected individual $(NH_4)_2V_6O_{16}\cdot 1.5H_2O$ nanobelts. The SAED pattern (Fig. 3b) shows clear diffraction spots, indicating a single crystal structure. The result from EDX shows (Fig. 3c) that the product contains only V, N, and O.

The effect of calcination on the crystallization and morphology of $(NH_4)_2V_6O_{16}\cdot 1.5H_2O$ was investigated. After calcination of $(NH_4)_2V_6O_{16}\cdot 1.5H_2O$ at 350 °C for 2 h, pure crystalline V_2O_5 was obtained. Fig. 4a and b shows representative low and high magnification SEM images of postcalcined V_2O_5 sample, indicating that the nest-like morphology of the precalcined $(NH_4)_2V_6O_{16}\cdot 1.5H_2O$ does not change after calcination. All the PXRD peaks shown in Fig. 4c could be readily indexed to the orthorhombic shcherbianite V_2O_5 phase (JCPDS Card no. 86-2248). The EDX spectrum analysis (inset of Fig. 4a) of V_2O_5 confirms that the product contains only V and O elements. The calcined sample was gold coated prior to the EDX analysis. The FTIR spectrum (Fig. 4d) of the calcined vanadium pentoxide is characterized by four absorption bands centered at 1028 cm^{-1}, 829 cm^{-1}, 630 cm^{-1} and 474 cm^{-1}. The first band at 1028 cm^{-1} is assigned to V=O stretching (Vanadyl oxygen) and the last three bands at 829 cm^{-1}, 630 cm^{-1} and 474 cm^{-1} are due to V–O–V deformation modes. The two bands at 3459 and 1642 cm^{-1} are attributed to O–H stretching and H–O–H bending vibrations of water molecules respectively [23].

The basic reactions for the formation of $(NH_4)_2V_6O_{16}\cdot 1.5H_2O$ phase can be tentatively proposed in a similar way as previously proposed for $Na_2V_6O_{16}\cdot 3H_2O$ [21].

$$3NH_4VO_3 + H_3PO_4 \rightarrow 3VO_3^- + (NH_4)_3PO_4 + 3H^+ \quad (1)$$

$$11VO_3^- + 8H^+ + H_2O \rightarrow [H_2V_{10}O_{28}]^{4-} + [VO_2(H_2O)_4] \quad (2)$$

$$[H_2V_{10}O_{28}]^{4-} + 4H^+ + 32H_2O \rightarrow 10[VO(OH)_3(H_2O)_2] \quad (3)$$

$$[VO_2(H_2O)_4]^+ \rightarrow [VO(OH)_3(H_2O)_2] + H^+ \quad (4)$$

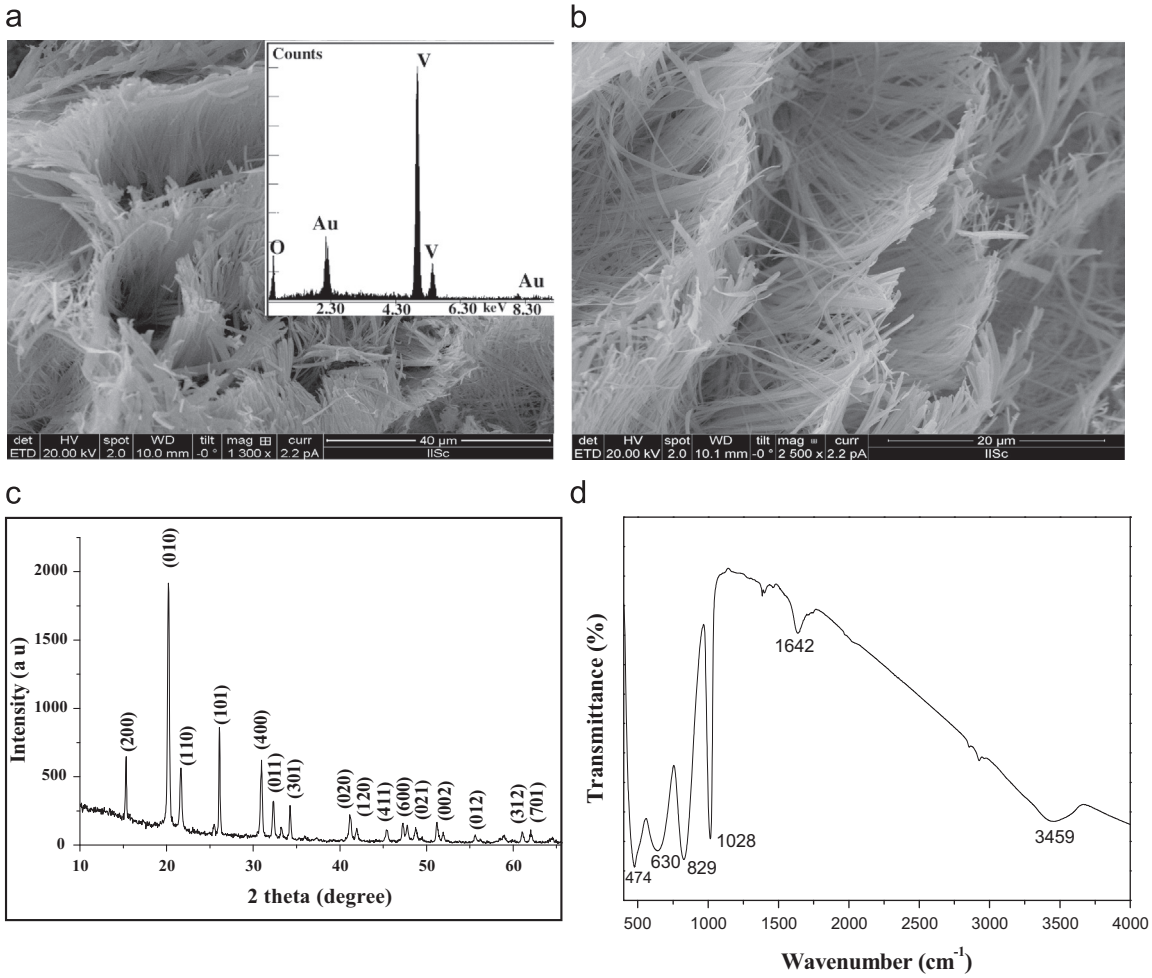

Fig.4. (a) and (b) SEM images (c) PXRD pattern and (d) FTIR spectrum of the calcined V_2O_5 product. Inset of a shows the EDX spectrum of V_2O_5 product.

$$6[VO(OH)_3(H_2O)_2] + 2NH_4^+ \rightarrow (NH_4)_2V_6O_{16}\cdot 1.5H_2O + 18.5H_2O + 2H^+ \quad (5)$$

In an aqueous solution, ammonium metavanadate forms NH_4^+ and VO_3^- ions. Addition of H_3PO_4 results in the formation of wine-red solution of vanadic acid (HVO_3) as shown in Eq. (1). The HVO_3 solution then progressively gets converted into a mixture of decavanadate $[H_2V_{10}O_{28}]^{4-}$ and $[VO_2(H_2O)_4]^+$ ions (Eq. (2)). The resulting solution was subjected to the hydrothermal treatment. During the reaction process, decavanadate $[H_2V_{10}O_{28}]^{4-}$ species get protonated (Eq. (3)) and the cationic $[VO_2(H_2O)_4]^+$ species undergoes deprotonation (Eq. (4)) in order to provide a neutral $[VO(OH)_3(H_2O)_2]$ precursor. Then, $(NH_4)_2V_6O_{16}\cdot 1.5H_2O$ (Eq. (5)) phase results from polycondensation of the neutral $[VO(OH)_3(H_2O)_2]$ precursor, leading to the formation of $V_3O_8^-$ layers, and the NH_4^+ ions can accommodate within these $V_3O_8^-$ framework tunnels in order to compensate for the negative charge of the layers.

The formation of $(NH_4)_2V_6O_{16}\cdot 1.5H_2O$ nanobelts can be explained in a similar manner as previously proposed for the formation of $Na_2V_6O_{16}\cdot 3H_2O$. Since these two compounds have a similar crystal structure and the same growth direction, the difference of these crystal structure parameters between $(NH_4)_2V_6O_{16}\cdot 1.5H_2O$ and $Na_2V_6O_{16}\cdot 3H_2O$ lies in the different length of the *c*-axis and the different β angles [24]. The $(NH_4)_2V_6O_{16}\cdot 1.5H_2O$ structure consists of $V_3O_8^-$ layers. NH_4^+ ions and water molecules are intercalated between these layers. During the hydrothermal process, the presence of anions plays an important role in the formation of nanobelts in a similar way as observed previously for the formation of vanadates [21]. Therefore, in the present work, we assume that the PO_4^{3-} anions are crucial for the growth of $(NH_4)_2V_6O_{16}\cdot 1.5H_2O$ nanobelts, because PO_4^{3-} has a stronger coordination ability and may adsorb selectively to the special crystal facets, leading to the formation of $(NH_4)_2V_6O_{16}\cdot 1.5H_2O$ belts. Further, the residual NH_4^+ ions from the solution could be escaped as NH_3 gas through the formation of bubbles and the $(NH_4)_2V_6O_{16}\cdot 1.5H_2O$ belts reside on the gas bubble. Finally, the bubble could be destroyed and leads to the formation of nest-like morphology. However, further study is needed to precisely understand the formation mechanism of the nest like morphology.

4. Conclusions

In conclusion, $(NH_4)_2V_6O_{16}\cdot 1.5H_2O$ nest-like morphology has been successfully prepared by the simple hydrothermal route. Nest-like morphology was formed due to the self-assembly of individual nanobelts. After calcination at 350 °C, $(NH_4)_2V_6O_{16}\cdot 1.5H_2O$ leads to pure crystalline V_2O_5.

Acknowledgments

The authors gratefully acknowledge the DST, New Delhi, India for financial support and Prof. Sarala Upadhya, UVCE, Bangalore for the SEM measurements.

References

[1] S. Shi, M. Cao, X. He, H. Xie, Cryst. Growth Des. 9 (2007) 1893.
[2] N. Wang, W. Chen, L.Q. Mai, Y. Dai, J. Solid State Chem. 181 (2008) 652.
[3] J.G. Yu, J.C. Yu, W.K. Ho, L. Wu, X.C. Wang, J. Am. Chem. Soc. 126 (2004) 3422.
[4] W. Chen, Q. Xu, Y.S. Hu, L.Q. Mai, Q.Y. Zhu, J. Mater. Chem. 12 (2002) 1926.
[5] J. Livage, Chem. Mater. 3 (1991) 578.
[6] Z. Huang, Z. Zhu, Z. Liu, Q. Liu, J. Catal. 214 (2003) 213.
[7] L.Q. Mai, W. Chen, Q. Xu, J.F. Peng, Q.Y. Zhu, Chem. Phys. Lett. 382 (2003) 307.
[8] J.F. Liu, X. Wang, Q. Peng, Y.D. Li, Adv. Mater. 17 (2005) 764.
[9] A.R. Raju, C.N.R. Rao, J. Chem. Soc. Chem. Commun. 18 (1991) 1260.
[10] I.H. Kim, J.H. Kim, B.W. Cho, Y.H. Lee, K.B. Kim, J. Electrochem. Soc. 153 (2006) A989.
[11] C.R. Xiong, A.E. Aliev, B. Gnade, K.J. Balkus, ACS Nano 2 (2008) 293.
[12] G.T. Chandrappa, P. Chithaiah, S. Ashoka, J. Livage, Inorg. Chem. 50 (2011) 7421.
[13] B.C. Satishkumar, A. Govindraj, M. Nath, C.N.R. Rao, J. Mater. Chem. 10 (2000) 2115.
[14] S. Myung, M. Lee, G.T. Kim, J.S. Ha, S.H. Hong, Adv. Mater. 17 (2005) 2361.
[15] G.T. Chandrappa, N. Steunou, S. Cassaignon, C. Bauvais, J. Livage, Catal. Today 78 (2003) 85.
[16] S.J. Park, J.S. Ha, Y.J. Chang, G.T. Kim, Chem. Phys. Lett. 390 (2004) 199.
[17] O. Durupthy, N. Steunou, T. Coradin, J. Maquet, C. Bonhomme, J. Livage, J. Mater. Chem. 15 (2005) 1090.
[18] J.G. Yu, J.C. Yu, W.K. Ho, L. Wu, X.C. Wang, J. Am. Chem. Soc. 126 (2004) 3422.
[19] G.T. Zhou, X.C. Wang, J.C. Yu, Cryst. Growth Des. 5 (2005) 969.
[20] L.Q. Mai, C.S. Lao, B. Hu, J. Zhou, Y.Y. Qi, W. Chen, E.D. Gu, Z.L. Wang, J. Phys. Chem. B 110 (2006) 8138.
[21] P. Chithaiah, G.T. Chandrappa, J. Livage, Inorg. Chem. 51 (2012) 2241.
[22] L. Jiao, H. Yuan, Y. Wang, J. Cao, Y. Wang, Electrochem. Commun. 7 (2005) 431.
[23] M. Gotic, S. Popovic, M. Ivanda, S. Music, Mater. lett. 57 (2003) 3190.
[24] Y. Xue, X. Zhang, J. Zhang, J. Wu, Y. Sun, Y. Tian, Y. Xie, J. Mater. Chem. 22 (2012) 2560.